MOLECULAR IMAGING AND BIOLOGY

Mol Imaging Biol (2019) 21:954–964
DOI: 10.1007/s11307-018-01304-3

Published Online: 22 January 2019

RESEARCH ARTICLE

Radiomics Analysis of PET and CT Components of PET/CT Imaging Integrated with Clinical Parameters: Application to Prognosis for Nasopharyngeal Carcinoma

Wenbing Lv,[1] Qingyu Yuan,[2] Quanshi Wang,[2] Jianhua Ma,[1] Qianjin Feng,[1] Wufan Chen,[1] Arman Rahmim,[3,4] Lijun Lu[1]

[1]*School of Biomedical Engineering and Guangdong Provincial Key Laboratory of Medical Image Processing, Southern Medical University, 1023 Shatai Road, Guangzhou, 510515, Guangdong, China*
[2]*Nanfang PET Center, Nanfang Hospital, Southern Medical University, 1023 Shatai Road, Guangzhou, 510515, Guangdong, China*
[3]*Department of Radiology, Johns Hopkins University, 601 N. Caroline St., Baltimore, MD, 21287, USA*
[4]*Departments of Radiology and Physics & Astronomy, University of British Columbia, 6224 Agricultural Road, Vancouver, BC, V6T 1Z1, Canada*

Abstract

Purpose: To investigate the prognostic performance of radiomics features, as extracted from positron emission tomography (PET) and X-ray computed tomography (CT) components of baseline 2-deoxy-2-[^{18}F]fluoro-D-glucose ([^{18}F]FDG) PET/CT images and integrated with clinical parameters, in patients with nasopharyngeal carcinoma (NPC).

Procedures: One hundred twenty-eight NPC patients (85 vs. 43 for training vs. validation), containing a subset of 86 patients with local-regional advanced stage, were enrolled. All patients underwent pretreatment PET/CT scans (mean follow-up time 24 ± 14 months). Three thousand two hundred seventy-six radiomics features extracted from PET or CT components and 13 clinical parameters were used to predict progression-free survival (PFS). Univariate analysis with Benjamini–Hochberg false discovery rate (FDR) correction was first used to screen significant features, and redundant features with Spearman's correlation >0.8 were further eliminated. Then, seven multivariate models involving PET features and/or CT features and/or clinical parameters (denoted as clinical, PET, CT, clinical + PET, clinical + CT, PET + CT and clinical + PET + CT) were constructed by forward stepwise multivariate Cox regression. Model performance was evaluated by concordance index (C-index).

Results: Sixty patients encountered events (28 recurrences, 17 metastases, and 15 deaths). Six clinical parameters, 3 PET features, and 14 CT features in training cohort and 4 clinical parameters, 10 PET features, and 4 CT features in subset of local-regional advanced stage were significantly associated with PFS. Combining PET and/or CT features with clinical parameters showed equal or higher prognostic performance than models with PET or CT or clinical parameters alone (C-index

Electronic supplementary material The online version of this article (https://doi.org/10.1007/s11307-018-01304-3) contains supplementary material, which is available to authorized users.

Correspondence to: Quanshi Wang; *e-mail:* wangquanshiwl@126.com, Jianhua Ma; *e-mail:* jhma@smu.edu.cn, Lijun Lu; *e-mail:* ljlubme@gmail.com

0.71–0.76 vs. 0.67–0.73 and 0.62–0.75 vs. 0.54–0.75 for training and validation cohorts, respectively), while the prognostic performance was significantly improved in local-regional advanced cohort (C-index 0.67–0.84 vs. 0.64–0.77, p value 0.001–0.059).
Conclusion: Radiomics features extracted from the PET and CT components of baseline PET/CT images provide complementary prognostic information and improved outcome prediction for NPC patients compared with use of clinical parameters alone.

Key words: Radiomics, Clinical parameter, Prognosis, [^{18}F]FDG PET/CT, Nasopharyngeal carcinoma

Introduction

Nasopharyngeal carcinoma (NPC) is a rare form of head and neck cancer worldwide, with high incidence in southern China; it occurs up to 30 per 100,000 persons annually [1]. Though improved radiotherapy or chemoradiotherapy has been applied in the past years, the 5-year progression-free survival rates of patients with advanced NPC remain around 60 % [2]. Outcome prediction is thus crucial to make more informed decisions regarding treatment [3]. For example, in high-risk patients, more aggressive treatment regimens and/or more intense monitoring can be administrated. Several clinical and histopathological measures have been identified as prognostic factors in NPC patients, including hemoglobin (HGB), platelet count (PLT) [4], serum lactate dehydrogenase level (LDH) [5], neutrophil count (NEUT) [6], and especially plasma Epstein–Barr virus DNA load (EBV-DNA) [7]. Nevertheless, exploring more precise and reliable prognostic factors still needs to be investigated [8].

2-Deoxy-2-[^{18}F]fluoro-D-glucose ([^{18}F]FDG) positron emission tomography (PET)/X-ray computed tomography (CT) imaging has been increasingly used in the management of patient with NPC and has been extensively exploited for TNM classification [9]. Image-based standardized uptake value (SUV) parameters and total lesion glycolysis (TLG) have been investigated as prognostic factors [10, 11]. As malignant tumors are commonly heterogeneous [12], quantitative description of intratumoral heterogeneity has shown significant potential for improved prognosis in various tumors [13–15]. Radiomics analysis, by extracting high-throughput features from tumor image, can provide important information regarding tumor heterogeneity [16]. As such, radiomics features derived from PET images have been explored as image-based biomarkers for improved diagnosis [17], prognosis [18–21], and treatment response assessment [12, 22, 23]. Besides, radiomics analysis on CT images also showed predictive and prognostic potential for head and neck cancer [24–26]. In the specific case of NPC, Law *et al.* investigated the value of skewness of the apparent diffusion coefficient (ADC) distribution curve from diffusion-weighted imaging (DWI) to predict local failure of NPC [27]. Huang *et al.* adopted the derivative of a volume threshold function for heterogeneity characterization and outcome prediction [13]. Chan *et al.* demonstrated that texture features were significantly associated with NPC survival while conventional PET metrics were not [28]. Zhang *et al.* conducted multiparametric MRI-based radiomics analysis to enhance the prognostic performance in advanced NPC [29]. Lv *et al.* found that radiomics features outperformed conventional metrics in the differentiation of NPC from chronic nasopharyngitis [17].

Despite the fact that both PET and CT images are generated by [^{18}F]FDG PET/CT imaging simultaneously, radiomics studies often focus on the PET component, while the CT component is commonly used to perform attenuation correction and tracer uptake localization. Nevertheless, the combined utilizations of PET and CT information for radiotherapy tumor response in lung cancer [30], radiation targeting in head and neck cancer [31, 32], and radiation pneumonitis diagnosis [33] have been investigated. Besides, some studies have demonstrated that radiomics analysis on the low-dose CT component of PET/CT can provide additional prognostic information compared to PET image features and/or clinical parameters, specifically for lymphomas [34] and non-small cell lung cancer [35–37]. To the best of our knowledge, prognostic analysis of NPC *via* radiomics features extracted from the PET and CT components of PET/CT (including integration of clinical parameters) has not been investigated. This study was to investigate extraction of pretreatment radiomics features from the PET and CT components, coupled with clinical parameters, as risk factors to evaluate prediction of outcome in NPC, aiming to improve prognostication and risk stratification of NPC patients.

Materials and Methods

Patients and PET/CT Imaging

This retrospective study was approved by the Institutional Review Board and informed consent was waived. One hundred twenty-eight patients (103 men and 25 women; mean age, 47.7 ± 13.2 years) primarily diagnosed with NPC with pathology confirmation were enrolled in this study (scan dates from January 2012 to August 2016). Two thirds of all patients (85 cases) were randomly selected for training purpose, and the remaining 43 patients were regarded as

validation cohort. A subset of 86 patients with local-regional advanced stage were also used for model construction.

All patients underwent a whole-body [^{18}F]FDG PET/CT scanning before treatment on a Biograph-128 mCT scanner (Siemens Healthineers, Erlangen, Germany) complying with the European Association of Nuclear Medicine (EANM) procedure guidelines [38]. An additional limited-area tumor imaging, *i.e.*, one bed position of nasopharynx for a few minutes, was also performed, and patients were encouraged to lie still in the PET/CT system for the duration of the examination to minimize motion blur. Patients were injected with 306–468 MBq (8.27–12.65 mCi) of [^{18}F]FDG depending on patient's weight (~ 150 μCi/kg of body weight) after fasted for 6 h, and PET/CT scanning was performed after about 60-min uptake (mean 58 ± 5 min, range 52–66 min). PET image reconstructions were finished by standard ordered subset expectation maximization (OSEM) (3 iterations, 21 subsets) and further converted to body weight SUVs for following analysis. CT images (80 mA, 120 kVp) with size of 512 × 512 were obtained for attenuation correction. PET image (voxel size 4.07 mm, slice thickness 5 mm) was then interpolated to the same resolution as CT image (voxel size 0.98 mm, slice thickness 3 mm) for registration/fusion purposes by cubic interpolation. Tumor delineation and radiomics feature extraction were thus conducted on the interpolated images.

Treatment and Follow-up

All patients received either radiotherapy or chemoradiotherapy; intensity-modulated radiation therapy (IMRT) was adopted; cisplatin-based chemotherapy was performed with 5-fluorouracil and/or docetaxel every 3 weeks. Progression-free survival (PFS), which is defined as the time from the day of primary treatment completion to the date of histological or imaging evidence for disease progression (local or regional recurrences or distant metastases), death from any cause, or the date of the last follow-up visit (censored), was selected as the main endpoint. All patients had a regular follow-up schedule every week during treatment, every 3 months during the first year after therapy, and 6 months thereafter. The mean follow-up time was 24 ± 14 months (range 1–56 months). Progression was assessed *via* clinical symptoms, physical examination, flexible nasopharyngoscopy, biopsy, or radiographic evidence (PET/CT, MRI, *et al.*).

Image Preprocessing

In order to characterize intratumor heterogeneity more comprehensively, a discrete, one-level, and undecimated 3D wavelet transform "Coiflet 1" was applied to each PET or CT image [39], by performing low-pass (L) or high-pass (H) filter along *x*-, *y*-, or *z*-directions, resulting in 8 decompositions of original image, noted as follows: LLL, LLH, LHL, LHH, HLL, HLH, HHL and HHH.

Two radiologists with 3 and 10 years of experience in interpreting nasopharyngeal PET/CT images delineated the 3D primary tumor on the fusion image of PET and CT by using the ITK-SNAP 3.4 software (www.itksnap.org), and the two showed high consistency with a median Dice similarity coefficient (DSC) of 0.87. Since features were found to be more robust to inter-observer variability compared to test-retest variability [40], we also found features were more robust with respect to multiple segmentation methods (including automatic and manual) than discretization in a previous study [41]. In the present work, the intersections of the two manual segmentations by the two radiologists were used for subsequent analysis.

Before feature extraction, original image and all decompositions were discretized to 32, 64, 128, and 256 different values. Since the applied wavelet decomposition is undecimated, the size of each decomposition is equal to the original image and each decomposition is shift invariant. As such, the original tumor delineation can be applied directly to the decomposition images. Thus, in total, we obtained $(8 + 1) \times 4 = 36$ kinds of feature extraction for each tumor.

Radiomics Features

Features were extracted in MATLAB R2016a (The MathWorks Inc.) using a package developed in-house based on an available radiomic analysis package (https://github.com/mvallieres/radiomics) [42]. We have extended the package and ensured that the definitions of features agree with the imaging biomarker standardization initiative (IBSI) [43], towards more reproducible research. Our package (corresponding to a previous publication [17]) has been made publicly available at https://github.com/WenbingLv/NPC-radiomics, which is continually expanding.

Our radiomics analysis included 9 shape features extracted from the segmentation mask, 19 SUV/HU features extracted on 9 VOIs ($19 \times 9 = 171$), and 86 texture features extracted on 9 VOIs (for PET or CT images) under 4 types of discretization ($86 \times 9 \times 4 = 3096$), arriving at 3276 total features. Of the 86 texture features, 57 are conventional texture features commonly appearing in the various literatures (including 26 features from gray-level co-occurrence matrix (GLCM), 13 features from gray-level run length matrix (GLRLM), 13 features from gray-level size zone matrix (GLSZM), and 5 features from neighborhood gray tone difference matrix (NGTDM)); we also introduced 29 uncommon texture features to fully explore intratumor heterogeneity (including 13 gray-level gap length matrix (GLGLM) features [44], 5 neighboring gray-level dependence matrix (NGLDM) features [45], 2 texture spectrum (TS) features, 3 texture feature coding (TFC) features, and 6 texture feature coding co-occurrence matrix (TFCM) features [46]). The various features are elaborated in the Supplemental Appendix A.

Clinical Parameters

Thirteen clinical parameters were obtained from the medical records. Specifically, age, sex, initial T, N, and M category, AJCC stage, pretreatment plasma EBV DNA, immunoglobulin A antibodies against EBV viral capsid antigen (VCA-IgA), lymphocyte count (LYM), neutrophil count (NEUT), hemoglobin (HGB), platelet count (PLT), and lactate dehydrogenase level (LDH) were evaluated in this study.

Statistical Analysis

Univariate Cox regression together with Benjamini–Hochberg false discovery rate (FDR) correction was first used to screen for significant features in the training cohort, and redundant features showed Spearman's correlation >0.8 were further eliminated. Thus, seven multivariate Cox regression models involved different combinations were then constructed: (1–3) use of clinical parameters or PET or CT features alone (denoted as clinical, PET, CT), (4–5) combining clinical parameters and PET features or CT features (denoted as clinical + PET, clinical + CT, respectively), (6) combining PET features and CT features (denoted as PET + CT), (7) integrating clinical parameters and PET features and CT features (denoted as clinical + PET + CT). Forward stepwise feature selection was utilized making use of a maximum log-likelihood (LOGL) criterion [47], noting that $2(\mathrm{LOGL}(\mathrm{model}_2)\text{-}\mathrm{LOGL}(\mathrm{model}_1))$ is approximately a chi-squared distribution with degree of freedom $(\mathrm{df}) = \mathrm{df}(\mathrm{model}_2)\text{-}\mathrm{df}(\mathrm{model}_1)$. Setting p value $= 0.05$ for accepting a new model_2 with an additional feature (degree of freedom) relative to model_1, then the new LOGL must be higher by >1.92. This turns out to be close to a required increase in LOGL by >2 as suggested for the effective parsimony information criterion (EPIC), which corresponds to a likelihood ratio test at level 0.05 when testing for the use of one additional feature between two models [48]. As such, features significantly increasing LOGL of the model were retained. Our criterion was thus more conservative compared to the Akaike information criterion (AIC), requiring LOGL increase by >1 only.

A prognostic score was generated for each multivariate Cox model by summing the products of each feature retained in the model and its corresponding regression coefficient (β) [15]. Patients were dichotomized into low- and high-risk groups by the median value of prognostic score; log-rank test was then used to compare the significant difference between two Kaplan–Meier curves. The same median value as used in training cohort in each model was applied to the validation cohort. The concordance index (C-index) was used to evaluate the discriminative power of each model. Significant difference between two C-indices was tested using the Hmisc R package.

Results

Patient Characteristics

The characteristics of 128 patients are summarized in Table 1. There were 15 patients with stages I–II and 113 patients with stages III–IV. The metabolically active tumor volume (MATV) of the 128 patients was 50.9 ± 86.4 (range 0.89–755.9 mm^3), SUVmax was 15.4 ± 7.77 (range 1.70–41.4), SUVmean was 7.95 ± 3.75 (range 1.07–21.4), and HUmean was 50.4 ± 55.1 (range -133.6–322.8). The mean follow-up time was 24 ± 14 months (range 1–56 months; median 23 months), and 60 patients had progression (28 recurrences, 17 metastases, and 15 deaths) by the last follow-up.

Fig. 1a–h showed four groups of patients with stages I, II, III, and IV, respectively, while patients with the same stage had distinct PFS, two patients with stage I having PFS of 21 *vs.* 52 months, stage II for 4 *vs.* 45 months, stage III for 6 *vs.* 43 months, and stage IV for 1 *vs.* 38 months.

Univariate Analysis for Prognostic Factor Screening

In univariate Cox proportional hazard regression analysis, after FDR correction and redundant feature elimination, 6 clinical parameters (M stage, age, VCA-IgA, AJCC stage, N stage, and LYM), 3 PET features (SUVmid_HLH, DiffVar_GLCM_LHH_128, and Variance_TFC_LHH_32), and 14 CT features were found to be significantly associated with PFS rates in training cohort, while 4 clinical parameters (PLT, AJCC stage, N stage, and VCA-IgA), 10 PET features, and 4 CT features (GLN_GLSZM_Im_256, GaLV_GLGLM_HHH_256, MaxPossibility_GLCM_Im_64, and Coarseness_TFC_LHL_256) were significantly associated with PFS in a subset of local-regional advanced stage. Corresponding p values, HR, and 95 % CI are detailed in Supplemental Appendix B Tables S1 and S2.

Multivariate Analysis for Model Construction

Features retained as independent prognostic factors for each model in training cohort are shown in Table 2. For models involving clinical parameters, M stage ($p < 0.006$) and VCA-IgA ($p < 0.023$) were consistently found to be significant predictors. For models involving CT radiomics features, GLV_GLSZM_LHH_256 consistently appeared with p values < 0.019. Meanwhile, no PET feature was retained when models involved PET features and clinical parameters and/or CT features, which means clinical + PET model is equal to clinical model and clinical + PET + CT model is equal to clinical + CT model.

Features retained as independent prognostic factors for each model in a subset of local-regional advanced stage are shown in Table 3. PLT ($p < 0.005$) and AJCC stage ($p <$

Table 1. Clinical characteristics of all patients, training cohort, validation cohort, and a subset patient of loco-regional advanced NPC

Characteristic	All patients	Training	Validation	Loco-regional advanced
Patient no.	128	85	43	86
Age (year), mean ± SD	47.7 ± 13.2	48.1 ± 13.9	47.9 ± 15.1	46.1 ± 13.5
Sex, no. (%)				
Male	103 (80.5 %)	67 (78.8 %)	36 (83.7 %)	65 (75.6 %)
Female	25 (19.5 %)	18 (21.2 %)	7 (16.3 %)	21 (24.4 %)
T stage, no. (%)				
T1	20 (15.6 %)	17 (20 %)	3 (6.9 %)	10 (11.6 %)
T2	20 (15.6 %)	14 (16.5 %)	6 (14 %)	10 (11.6 %)
T3	54 (42.3 %)	34 (40 %)	20 (46.5 %)	42 (48.8 %)
T4	34 (26.5 %)	20 (23.5 %)	14 (32.6 %)	24 (28.0 %)
N stage, no. (%)				
N0	14 (10.9 %)	10 (11.8 %)	4 (9.3 %)	6 (7.0 %)
N1	33 (25.8 %)	20 (23.5 %)	13 (30.2 %)	22 (25.6 %)
N2	54 (42.2 %)	36 (43.4 %)	18 (41.9 %)	43 (50.0 %)
N3	27 (21.1 %)	19 (22.3 %)	8 (18.6 %)	15 (17.4 %)
M stage, no. (%)				
M0	101 (78.9 %)	70 (82.3 %)	31 (72.1 %)	86 (100 %)
M1	27 (21.1 %)	15 (17.7 %)	12 (27.9 %)	0 (0 %)
AJCC stage, no. (%)				
I	4 (3.1 %)	2 (2.4 %)	2 (4.7 %)	0 (0 %)
II	11 (8.6 %)	8 (9.4 %)	3 (6.9 %)	0 (0 %)
III	51 (39.8 %)	34 (40.0 %)	17 (39.6 %)	51 (59.3 %)
IV	62 (48.5 %)	41 (48.2 %)	21 (48.8 %)	35 (40.7 %)
MATV	50.9 ± 86.4	45.1 ± 67.8	62.2 ± 114.9	56.0 ± 90.9
SUVmax	15.4 ± 7.77	14.0 ± 7.26	18.2 ± 8.08	16.1 ± 7.57
SUVmean	7.95 ± 3.75	7.15 ± 3.24	9.54 ± 4.19	8.14 ± 3.57
HUmean	50.4 ± 55.1	43.8 ± 54.1	63.4 ± 55.4	44.1 ± 46.1
Follow-up time, mean ± SD (months)	24 ± 14	24 ± 14	24 ± 14	27 ± 13
Follow-up time, median (range)	23 (1–56)	22 (1–56)	25 (4–52)	26 (1–56)
Recurrence	28 (21.9 %)	19 (22.4 %)	9 (20.9 %)	19 (22.1 %)
Metastasis	17 (13.3 %)	12 (14.1 %)	5 (11.6 %)	16 (18.6 %)
Death	15 (11.8 %)	9 (10.6 %)	6 (13.9 %)	0 (0 %)

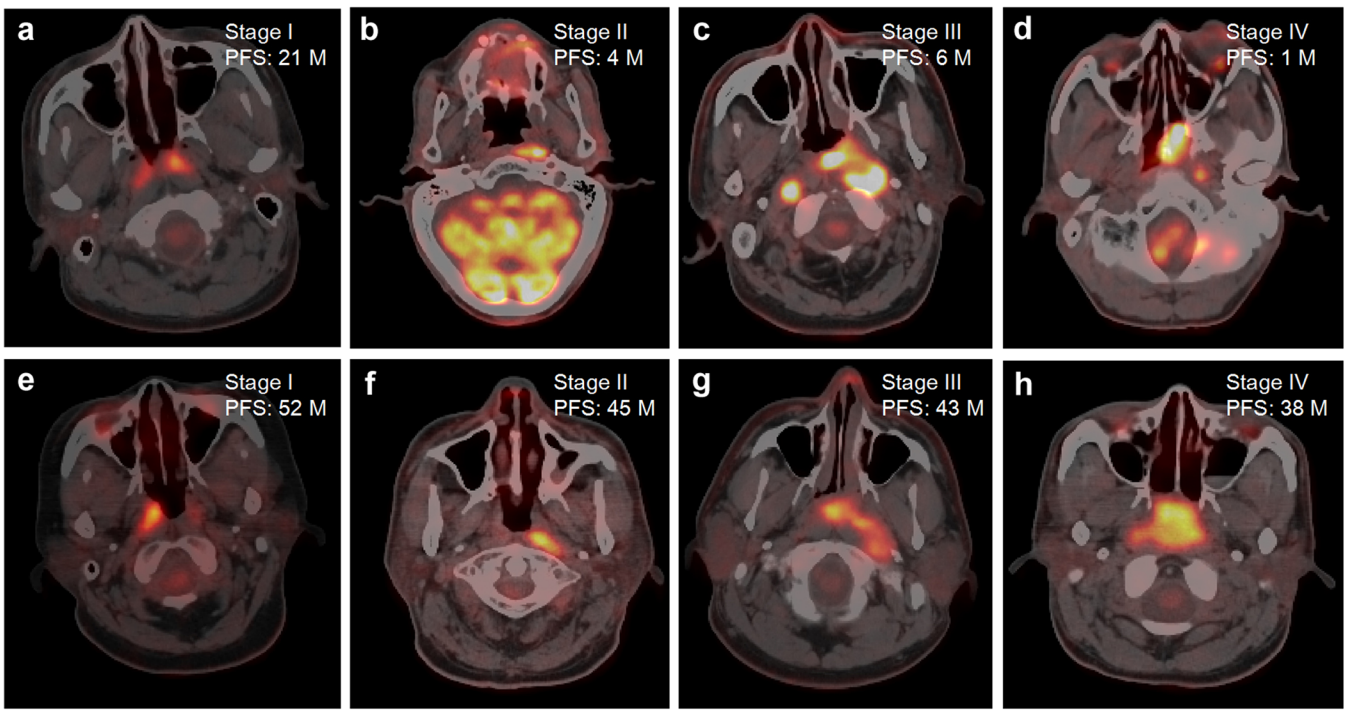

Fig. 1. The AJCC stage and progression-free survival (PFS) of eight representative patients. **a**, **e** Two patients with stage I; their PFS were 21 *vs.* 52 months. **b**, **f** Two patients with stage II; their PFS were 4 *vs.* 45 months. **c**, **g** Two patients with stage III; their PFS were 6 *vs.* 43 months. **d**, **h** Two patients with stage IV; their PFS were 1 *vs.* 38 months.

Table 2. Multivariate Cox regression analysis for each model in training cohort

Model	*p* value
Clinical	
"M stage"	0.006
"AJCC stage"	0.156
"VCA-IgA"	0.013
PET	
"SUVmid_HLH"	0.005
CT	
"Homogeneity_GLCM_LHH_128"	0.013
"LGGE_GLGLM_LLH_128"	0.007
"RLV_GLRLM_HLH_32"	0.040
"Complexity_NGTDM_LLH_256"	0.041
Clinical + PET	
Clinical parameters	
"M stage"	0.006
"AJCC stage"	0.156
"VCA-IgA"	0.013
PET features	None
Clinical + CT	
Clinical parameters	
"M stage"	0.001
"Age"	0.088
"VCA_IgA"	0.023
"N stage"	0.068
CT features	
"GLV_GLSZM_LHH_256"	0.019
PET + CT	
PET features	
"SUVmid_HLH"	< 0.001
CT features	
"SRHGE_GLRLM_LHL_128"	0.117
"LGGE_GLGLM_LLH_128"	0.002
"RLV_GLRLM_HLH_32"	0.007
"GLV_GLSZM_LHH_256"	0.011
Clinical + PET + CT	
Clinical parameters	
"M stage"	0.001
"Age"	0.088
"VCA_IgA"	0.023
"N stage"	0.068
PET features	None
CT features	
"GLV_GLSZM_LHH_256"	0.019

Table 3. Multivariate Cox regression analysis for each model in a subset with local-regional advanced stage

Model	*p* value
Clinical	
"PLT"	< 0.001
"AJCC stage"	0.001
PET	
"GLV_GLSZM_HLL_32"	0.015
"Coarseness_TFC_HLL_256"	0.001
"LGLGE_GLGLM_LHL_64"	0.006
CT	
"GLN_GLSZM_Im_256"	< 0.001
"MaxPossibility_GLCM_Im_64"	0.030
Clinical + PET	
Clinical parameters	
"PLT"	0.005
"AJCC stage"	< 0.001
PET features	
"GLV_GLSZM_HLL_32"	0.007
"SUVvar_HHL"	0.001
"Coarseness_TFC_HLL_256"	0.006
Clinical + CT	
Clinical parameters	
"PLT"	0.001
"AJCC stage"	< 0.001
CT features	
"GLN_GLSZM_Im_256"	0.020
"GaLV_GLGLM_HHH_256"	0.012
PET + CT	
PET features	
"RLV_GLRLM_HLL_128"	0.237
"Coarseness_TFC_HLL_256"	0.026
CT features	
"GLN_GLSZM_Im_256"	< 0.001
Clinical + PET + CT	
Clinical parameters	
"PLT"	0.001
"AJCC stage"	0.001
PET features	
"GLV_GLSZM_HLL_32"	0.021
"SUVvar_HHL"	< 0.001
"Coarseness_TFC_HLL_256"	< 0.001
CT features	
"GLN_GLSZM_Im_256"	0.001
"GaLV_GLGLM_HHH_256"	0.039

0.001) were consistently found to be significant predictors. Coarseness_TFC_HLL_256 ($p < 0.026$) from PET and GLN_GLSZM_Im_256 ($p < 0.020$) from CT were also consistently retained.

Model Performance

The C-index for each model is listed in Table 4. The C-index ranges of models with clinical parameters or PET or CT features alone are 0.67–0.73 and 0.54–0.75 for training and validation cohorts, respectively. Combining clinical parameters and/or PET and/or CT features showed equal or higher C-index than models without different kinds of feature combination (0.71–0.76 *vs.* 0.67–0.73 and 0.62–0.75 *vs.* 0.54–0.75 for training and validation cohorts, respectively). Kaplan–Meier curves of PFS rates of each model in training and validation patients are shown in Fig. 2. Since clinical + PET model is equal to clinical model and clinical + PET + CT model is equal to clinical + CT model, the Kaplan–Meier curves of clinical + PET model and clinical + PET + CT model were not shown.

As for the subset of local-regional advanced stage, clinical + PET + CT model showed significantly higher C-index of 0.84 than any other six models (C-index 0.64–0.81, *p* value 0.018–0.035); clinical + PET model (0.80) and clinical + CT model (0.81) also showed significantly higher C-index than models with PET or CT or clinical parameters alone (C-index 0.64–0.77, *p* value 0.001–0.028). Detailed significant difference comparisons (*p* value) of C-indices between different models are provided in Supplemental Appendix B Table S3. Kaplan–Meier curves of PFS rates of each model in the subset are shown in Fig. 3.

The prognostic score of clinical + PET + CT model *versus* survival time (PFS) on the subset patients is shown in Fig. 4. With survival time increasing, prognostic score shows a decreasing trend. The median prognostic score of 4.67 can better split them into high- or low-risk groups than AJCC stage.

Table 4. C-index and log-rank test *p* value for each model as applied to training, validation, and a subset with local-regional advanced stage cohorts

Model	Training		Validation		Local-regional advanced	
	C-index	*p* value	C-index	*p* value	C-index	*p* value
Clinical	0.71	0.001	0.75	0.016	0.77	9.06e−04
PET	0.67	0.025	0.62	0.025	0.66	9.97e−04
CT	0.73	0.002	0.54	0.855	0.64	0.037
Clinical + PET	0.71	0.001	0.75	0.016	0.80	3.97e−05
Clinical + CT	0.75	6.47e−06	0.75	0.004	0.81	1.16e−05
PET + CT	0.76	2.61e−05	0.62	0.010	0.67	0.013
Clinical + PET + CT	0.75	6.47e−06	0.75	0.004	0.84	4.08e−06

Discussion

We investigated the prognostic performance of radiomics features extracted from both PET and CT components of baseline PET/CT images integrated with clinical parameters in patients with NPC, and derived improved outcome prediction for NPC patients compared with use of clinical parameters or PET or CT features alone in both training and validation cohorts and a subset with local-regional advanced stage.

Models integrating PET and/or CT features with clinical parameters resulted in equal or higher prognostic performance with limited significance relative to models with PET or CT or clinical parameters alone (C-index 0.71–0.76 *vs.* 0.67–0.73 and 0.62–0.75 *vs.* 0.54–0.75 for training and validation cohorts, respectively; Table 4), while the prognostic performance was more obviously improved in local-regional advanced cohort (C-index 0.67–0.84 *vs.* 0.64–0.77, *p* value 0.001–0.059; Table 4; Supplemental Appendix B Table S3) as focused in [29]. Since features showed

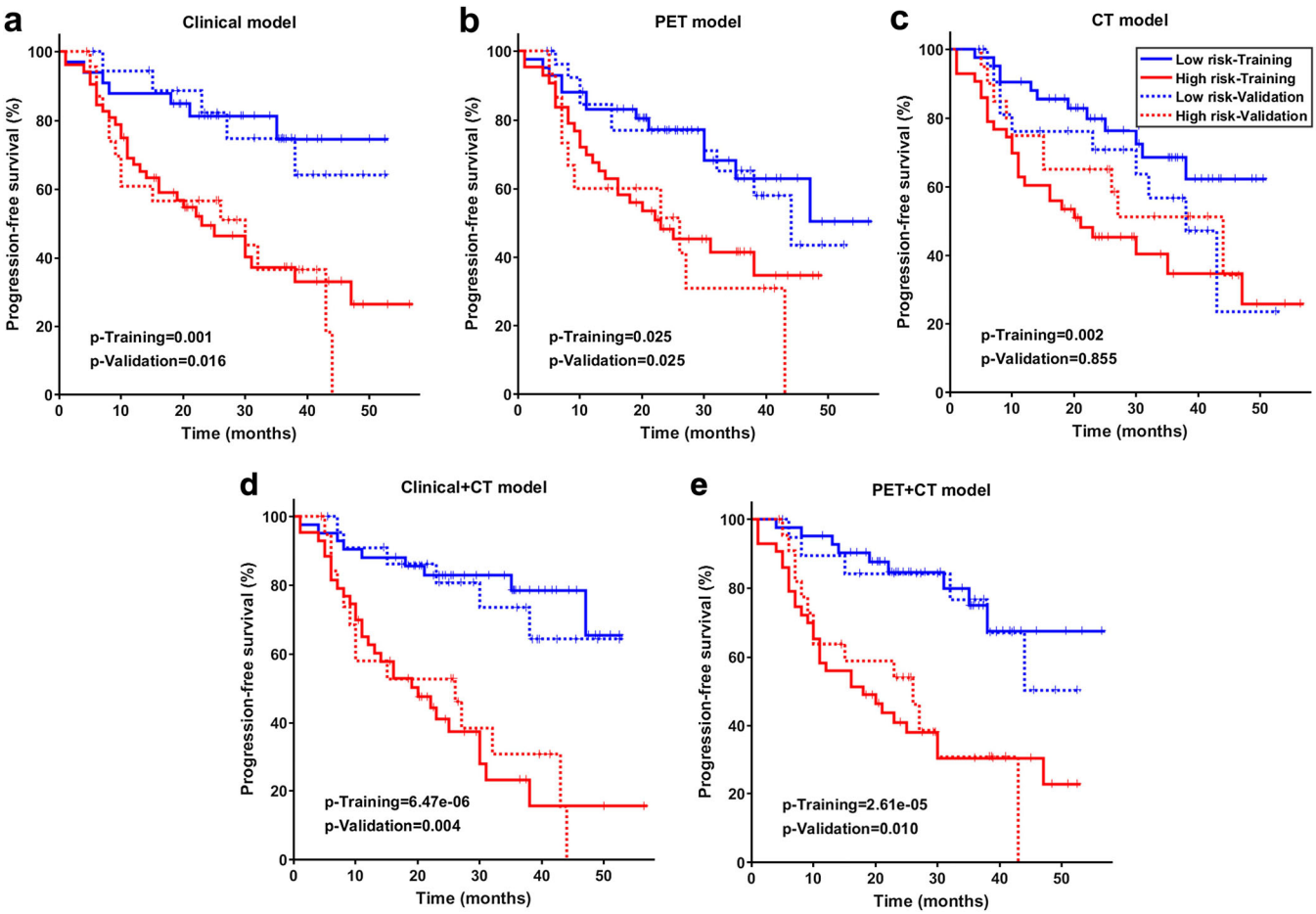

Fig. 2. Kaplan–Meier curves of PFS rates for training ($n = 85$) and validation patients ($n = 43$), showing **a** clinical model, **b** PET model, **c** CT model, **e** clinical + CT model, and **f** PET + CT model. Since clinical + PET model is equal to clinical model and clinical + PET + CT model is equal to clinical + CT model, the Kaplan–Meier curves of clinical + PET model and clinical + PET + CT model were not shown.

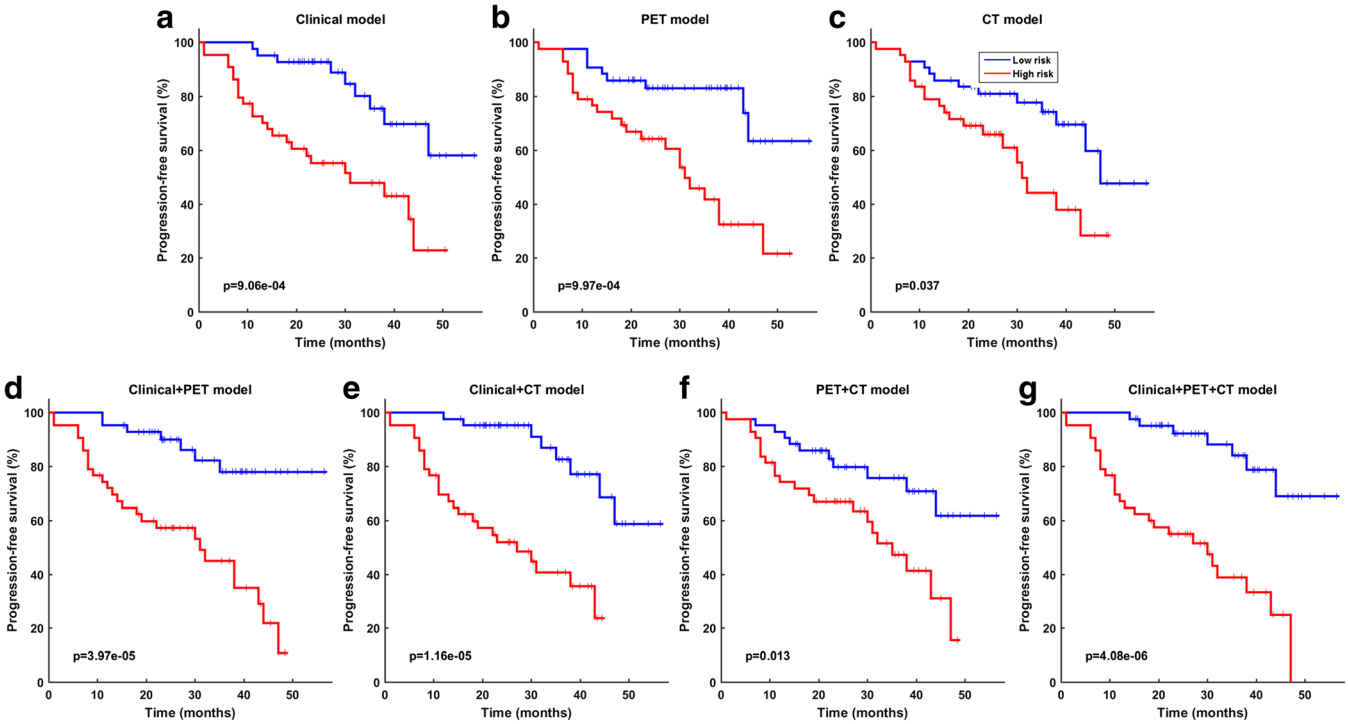

Fig. 3. Kaplan–Meier curves of PFS rates for a subset with local-regional advanced stage cohorts ($n = 86$), showing **a** clinical model, **b** PET model, **c** CT model, **d** clinical + PET model, **e** clinical + CT model, **f** PET + CT model, and **g** clinical + PET + CT model.

Spearman's correlation higher than 0.8 were pre-eliminated, features retained in all models were weakly correlated with one another. As such, the information provided by different features was non-redundant with respect to one another, and comprehensive tumor characterization using both PET and CT images could add value to the use of clinical parameters alone.

An interesting finding was that the prognostic performance of the CT model (C-index 0.73) was superior to that of the PET model (C-index 0.67, $p = 0.035$) in the training cohort, while it was reversed in the validation (C-index 0.54 *vs.* 0.62, $p = 0.043$) and subset cohorts (C-index 0.64 *vs.* 0.66 for CT and PET respectively, $p = 0.074$) (Table 4). It is worth pointing out that the VOIs were delineated on the PET/CT fusion images. Overall, PET images may provide better visualization for radiologists and reveal the glucose metabolism information, while CT images have higher resolution than PET and convey the anatomic characteristic, such as vascularization, edema, and necrosis. To ascertain the relative contributions of PET and CT features on the characterization of intratumor heterogeneity, significantly larger cohorts within more standardized procedure [49] may need to be investigated.

The significant features retained in each model were not extracted from the original image but from different wavelet decomposition images (Tables 2 and 3) as investigated in other literatures [21, 39, 50–52], indicating that wavelet decomposition images may better reveal inconspicuous prognostic

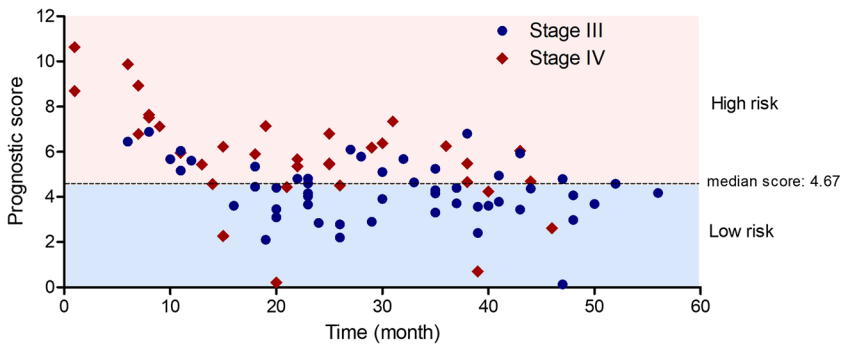

Fig. 4. Plot of the prognostic score (clinical + PET + CT model) *versus* the survival time (PFS) of the subset with local-regional advanced stage. Stage III and IV patients are colored by blue and red, respectively.

information than original images. Besides, most features extracted from different wavelet decompositions were weakly correlated except GLN_GLSZM_256 from CT (Supplemental Appendix B Fig. S1), which means specific features are useful when only extracted from specific wavelet decomposition. Though multivariate models demonstrated that different features were significant for discretization bins, ranging from 32 to 256 (Tables 2 and 3), it is important to note that most features extracted from different discretization are highly correlated except GLV_GLSZM_HLL from PET (median Spearman's correlation 0.62) and RLV_GLRLM_HLH from CT (median Spearman's correlation 0.51) (Supplemental Appendix B Fig. S2). Thus, some features extracted from other discretization which are not retained are still useful, but there are alternatives among them. With regard to features with weak correlations among different discretization, it is essential to investigate optimal discretization bins, as evaluated in other applications in terms of performance [53–55], repeatability [56], and reproducibility/robustness [41, 57, 58].

The time of feature extraction was about tens of seconds, while the time of model training and validation was few seconds since only a subset of features were useful. The code can be further optimized to accelerate the computation. Therefore, it is acceptable for potential clinical application.

In order to validate the usefulness of previous reported features in our NPC cohorts, four features (energy, compactness, GLN_GLRLM, and GLN_GLRLM_HLH, noted as comparator 1) reported by Aerts et al. [39] and Leijenaar et al. [26] were first tested. However, none of them were found to be significantly associated with PFS on CT images in our training cohort (Supplemental Appendix B Table S4, Fig. S3a) [59]. Another three features (LGHGE_GLSZM_HHH, SumEntropy_GLCM_LLL, and DiffVar_GLCM_LLH, noted as comparator 2) reported by Bogowicz et al. [25] were also tested. The results were not satisfactory neither (Supplemental Appendix B Table S4, Fig. S3b), possibly because four tumor sites (oropharynx, hypopharynx, larynx, and oral cavity) were included in their study.

Our study had some limitations. First, a single survival endpoint (PFS) with short follow-up time that merges death, recurrence, and distant metastases together may confuse oncologists about the failure pattern of NPC patients. The inconsistent results between the two comparators and our study also emphasize the establishment of radiomics signatures with specific oncologic functions and endpoints [60], and thus, more endpoints with a larger number of patients per endpoint need to be investigated in the future. Profound understanding of biology meaning behind features is also needed to enable successful clinical transformation. Second, due to its retrospective nature and small size cohort from one institution, prospective larger cohort with external validation *via* a multicenter study [61] is necessary to confirm our results and improve the reliability of our radiomics study, which will enhance clinical application of prognostic signatures. Third, unenhanced CT component instead of contrast-enhanced diagnostic CT was used to extract features; the information of anatomical structure may not be substantially captured. Furthermore, the 3D tumor was delineated on fused images instead of on PET and CT components separately, which will confuse their relative contribution. Finally, directionally orientated wavelet decomposition may be affected by variations in the orientation of the head and neck during imaging.

Conclusion

Radiomics features were extracted from the PET and CT components of baseline PET/CT, quantitatively characterizing intratumor heterogeneity, and were shown to provide complementary prognostic information for NPC patients. Combining PET and/or CT features with clinical parameters showed improved outcome prediction relative to models with PET or CT radiomics features or clinical parameters alone in both training and validation cohorts, especially in local-regional advanced subset. It was also shown that radiomics features extracted from different wavelet decompositions could characterize the intratumor heterogeneity more accurately and further improve prognostic performance.

Funding Information. This work was supported by the National Natural Science Foundation of China under grants 61628105, 81501541, 81871437, U1708261, and 61471188, the National Key Research and Development Program under grant 2016YFC0104003, the Natural Science Foundation of Guangdong Province under grant 2016A030313577, the Program of Pearl River Young Talents of Science and Technology in Guangzhou under grant 201610010011, the Guangdong Province Universities and Colleges Pearl River Scholar Funded Scheme (Lijun Lu, 2018), and the China Scholarship Council under grant 201808440464.

Compliance with Ethical Standards

Conflict of Interest

The authors declare that they have no conflict of interest.

References

1. Wei WI, Sham JS (2005) Nasopharyngeal carcinoma. Lancet 365:2041–2054
2. Lee AWM, Tung SY, Chua DTT, Ngan RKC, Chappell R, Tung R, Siu L, Ng WT, Sze WK, Au GKH, Law SCK, O'Sullivan B, Yau TK, Leung TW, Au JSK, Sze WM, Choi CW, Fung KK, Lau JT, Lau WH (2010) Randomized trial of radiotherapy plus concurrent-adjuvant chemotherapy vs radiotherapy alone for regionally advanced nasopharyngeal carcinoma. J Natl Cancer Inst 102:1188–1198
3. Caponigro F, Longo F, Ionna F, Perri F (2010) Treatment approaches to nasopharyngeal carcinoma: a review. Anti-Cancer Drug 21:471–477
4. Chang H, Gao J, Xu BQ, Guo SP, Lu RB, Li G, Huang SM, Han F, Liu ZG, Tao YL, Tu ZW, Chen C, Li XH, Xia YF (2013) Haemoglobin, neutrophil to lymphocyte ratio and platelet count improve prognosis prediction of the TNM staging system in nasopharyngeal carcinoma: development and validation in 3,237 patients from a single institution. Clin Oncol 25:639–646
5. Wan XB, Wei L, Li H, Dong M, Lin Q, Ma XK, Huang PY, Wen JY, Li X, Chen J, Ruan DY, Lin ZX, Chen ZH, Liu Q, Wu XY, Hong MH

(2013) High pretreatment serum lactate dehydrogenase level correlates with disease relapse and predicts an inferior outcome in locally advanced nasopharyngeal carcinoma. Eur J Cancer 49:2356–2364
6. Zhong L, Li C, Ren Y, Wu D (2017) Prognostic value of 18F-fluorodeoxyglucose PET parameters and inflammation in patients with nasopharyngeal carcinoma. Oncol Lett 14:5004–5012
7. Wang WY, Twu CW, Chen HH et al (2013) Long-term survival analysis of nasopharyngeal carcinoma by plasma Epstein-Barr virus DNA levels. Cancer-Am Cancer Soc 119:963–970
8. Lee AW, Ma BB, Ng WT, Chan AT (2015) Management of nasopharyngeal carcinoma: current practice and future perspective. J Clin Oncol 33:3356–3364
9. Zhou H, Shen G, Zhang W, Cai H, Zhou Y, Li L (2016) ^{18}F-FDG PET/CT for the diagnosis of residual or recurrent nasopharyngeal carcinoma after radiotherapy: a metaanalysis. J Nucl Med 57:342–347
10. Chan SC, Chang JT, Lin CY, Ng SH, Wang HM, Liao CT, Chang CJ, Lin SY, Yen TC (2011) Clinical utility of ^{18}F-FDG PET parameters in patients with advanced nasopharyngeal carcinoma: predictive role for different survival endpoints and impact on prognostic stratification. Nucl Med Commun 32:989–996
11. Chang KP, Tsang NM, Liao CT, Hsu CL, Chung MJ, Lo CW, Chan SC, Ng SH, Wang HM, Yen TC (2012) Prognostic significance of ^{18}F-FDG PET parameters and plasma Epstein-Barr virus DNA load in patients with nasopharyngeal carcinoma. J Nucl Med 53:21–28
12. O'Connor JP, Rose CJ, Waterton JC et al (2015) Imaging intratumor heterogeneity: role in therapy response, resistance, and clinical outcome. Clin Cancer Res 21:249–257
13. Huang B, Chan T, Kwong DL et al (2012) Nasopharyngeal carcinoma: investigation of intratumoral heterogeneity with FDG PET/CT. AJR Am J Roentgenol 199:169–174
14. Cheng NM, Fang YH, Chang JT et al (2013) Textural features of pretreatment ^{18}F-FDG PET/CT images: prognostic significance in patients with advanced T-stage oropharyngeal squamous cell carcinoma. J Nucl Med 54:1703–1709
15. Foley KG, Hills RK, Berthon B, Marshall C, Parkinson C, Lewis WG, Crosby TDL, Spezi E, Roberts SA (2018) Development and validation of a prognostic model incorporating texture analysis derived from standardised segmentation of PET in patients with oesophageal cancer. Eur Radiol 28:428–436
16. Parekh V, Jacobs MA (2016) Radiomics: a new application from established techniques. Expert Rev Precis Med Drug Dev 1:207–226
17. Lv W, Yuan Q, Wang Q, Ma J, Jiang J, Yang W, Feng Q, Chen W, Rahmim A, Lu L (2018) Robustness versus disease differentiation when varying parameter settings in radiomics features: application to nasopharyngeal PET/CT. Eur Radiol 28:3245–3254
18. Lovinfosse P, Polus M, Van Daele D et al (2018) FDG PET/CT radiomics for predicting the outcome of locally advanced rectal cancer. Eur J Nucl Med Mol Imaging 45:365–375
19. Chen SW, Shen WC, Lin YC, Chen RY, Hsieh TC, Yen KY, Kao CH (2017) Correlation of pretreatment (18)F-FDG PET tumor textural features with gene expression in pharyngeal cancer and implications for radiotherapy-based treatment outcomes. Eur J Nucl Med Mol Imaging 44:567–580
20. Yu W, Tang C, Hobbs BP et al (2017) Development and validation of a predictive radiomics model for clinical outcomes in stage I non-small cell lung cancer. Int J Radiat Oncol Biol Phys 102:1090–1097
21. Coroller TP, Grossmann P, Hou Y, Rios Velazquez E, Leijenaar RTH, Hermann G, Lambin P, Haibe-Kains B, Mak RH, Aerts HJWL (2015) CT-based radiomic signature predicts distant metastasis in lung adenocarcinoma. Radiother Oncol 114:345–350
22. Kickingereder P, Gotz M, Muschelli J et al (2016) Large-scale radiomic profiling of recurrent glioblastoma identifies an imaging predictor for stratifying anti-angiogenic treatment response. Clin Cancer Res 22:5765–5771
23. Tixier F, Le Rest CC, Hatt M et al (2011) Intratumor heterogeneity characterized by textural features on baseline ^{18}F-FDG PET images predicts response to concomitant radiochemotherapy in esophageal cancer. J Nucl Med 52:369–378
24. Ou D, Blanchard P, Rosellini S, Levy A, Nguyen F, Leijenaar RTH, Garberis I, Gorphe P, Bidault F, Ferté C, Robert C, Casiraghi O, Scoazec JY, Lambin P, Temam S, Deutsch E, Tao Y (2017) Predictive and prognostic value of CT based radiomics signature in locally advanced head and neck cancers patients treated with concurrent chemoradiotherapy or bioradiotherapy and its added value to human papillomavirus status. Oral Oncol 71:150–155
25. Bogowicz M, Riesterer O, Ikenberg K, Stieb S, Moch H, Studer G, Guckenberger M, Tanadini-Lang S (2017) Computed tomography radiomics predicts HPV status and local tumor control after definitive radiochemotherapy in head and neck squamous cell carcinoma. Int J Radiat Oncol Biol Phys 99:921–928
26. Leijenaar RT, Carvalho S, Hoebers FJ et al (2015) External validation of a prognostic CT-based radiomic signature in oropharyngeal squamous cell carcinoma. Acta Oncol 54:1423–1429
27. Law BK, King AD, Bhatia KS et al (2016) Diffusion-weighted imaging of nasopharyngeal carcinoma: can pretreatment DWI predict local failure based on long-term outcome? AJNR Am J Neuroradiol 37:1706–1712
28. Chan SC, Chang KP, Fang YD et al (2017) Tumor heterogeneity measured on F-18 fluorodeoxyglucose positron emission tomography/computed tomography combined with plasma Epstein-Barr virus load predicts prognosis in patients with primary nasopharyngeal carcinoma. Laryngoscope 127:E22–E28
29. Zhang B, Tian J, Dong D, Gu D, Dong Y, Zhang L, Lian Z, Liu J, Luo X, Pei S, Mo X, Huang W, Ouyang F, Guo B, Liang L, Chen W, Liang C, Zhang S (2017) Radiomics features of multiparametric MRI as novel prognostic factors in advanced nasopharyngeal carcinoma. Clin Cancer Res 23:4259–4269
30. Vaidya M, Creach KM, Frye J, Dehdashti F, Bradley JD, el Naqa I (2012) Combined PET/CT image characteristics for radiotherapy tumor response in lung cancer. Radiother Oncol 102:239–245
31. Yu H, Caldwell C, Mah K, Poon I, Balogh J, MacKenzie R, Khaouam N, Tirona R (2009) Automated radiation targeting in head-and-neck cancer using region-based texture analysis of PET and CT images. Int J Radiat Oncol Biol Phys 75:618–625
32. Yu H, Caldwell C, Mah K, Mozeg D (2009) Coregistered FDG PET/CT-based textural characterization of head and neck cancer for radiation treatment planning. IEEE Trans Med Imaging 28:374–383
33. Anthony GJ, Cunliffe A, Castillo R, Pham N, Guerrero T, Armato SG III, al-Hallaq HA (2017) Incorporation of pre-therapy F-18-FDG uptake data with CT texture features into a radiomics model for radiation pneumonitis diagnosis. Med Phys 44:3686–3694
34. Ganeshan B, Miles KA, Babikir S, Shortman R, Afaq A, Ardeshna KM, Groves AM, Kayani I (2017) CT-based texture analysis potentially provides prognostic information complementary to interim FDG-PET for patients with Hodgkin's and aggressive non-Hodgkin's lymphomas. Eur Radiol 27:1012–1020
35. Kirienko M, Cozzi L, Antunovic L, Lozza L, Fogliata A, Voulaz E, Rossi A, Chiti A, Sollini M (2018) Prediction of disease-free survival by the PET/CT radiomic signature in non-small cell lung cancer patients undergoing surgery. Eur J Nucl Med Mol Imaging 45:207–217
36. Desseroit MC, Visvikis D, Tixier F, et al (2016) Development of a nomogram combining clinical staging with ^{18}F-FDG PET/CT image features in non-small-cell lung cancer stage I-III. Eur J Nucl Med Mol Imaging 43:1477–1485
37. Win T, Miles KA, Janes SM, Ganeshan B, Shastry M, Endozo R, Meagher M, Shortman RI, Wan S, Kayani I, Ell PJ, Groves AM (2013) Tumor heterogeneity and permeability as measured on the CT component of PET/CT predict survival in patients with non-small cell lung cancer. Clin Cancer Res 19:3591–3599
38. Boellaard R, Delgado-Bolton R, Oyen WJG, et al (2015) FDG PET/CT: EANM procedure guidelines for tumour imaging: version 2.0. Eur J Nucl Med Mol I(42):328–354
39. Aerts HJWL, Velazquez ER, Leijenaar RTH, Parmar C, Grossmann P, Carvalho S, Bussink J, Monshouwer R, Haibe-Kains B, Rietveld D, Hoebers F, Rietbergen MM, Leemans CR, Dekker A, Quackenbush J, Gillies RJ, Lambin P (2014) Decoding tumour phenotype by noninvasive imaging using a quantitative radiomics approach. Nat Commun 5:4006
40. Leijenaar RT, Carvalho S, Velazquez ER et al (2013) Stability of FDG-PET Radiomics features: an integrated analysis of test-retest and inter-observer variability. Acta Oncol 52:1391–1397
41. Lu L, Lv W, Jiang J, Ma J, Feng Q, Rahmim A, Chen W (2016) Robustness of radiomic features in [^{11}C]choline and [^{18}F]FDG PET/CT imaging of nasopharyngeal carcinoma: impact of segmentation and discretization. Mol Imaging Biol 18:935–945

42. Vallieres M, Freeman CR, Skamene SR, El NI (2015) A radiomics model from joint FDG-PET and MRI texture features for the prediction of lung metastases in soft-tissue sarcomas of the extremities. Phys Med Biol 60:5471–5496
43. Zwanenburg A, Leger S, Vallières M, Löck S (2018) Image biomarker standardisation initiative. arXiv preprint arXiv:1612.07003v7
44. Wang X, Fritz A, Bent F (1994) Texture features from gray level gap length matrix. IAPR Workshop Mach Vision Appl [abstract] 8: 375–378
45. Sun C, Wee WG (1982) Neighboring gray level dependence matrix for texture classification. Comput Vision Graph 23:341–352
46. Horng MH, Sun YN, Lin XZ (2002) Texture feature coding method for classification of liver sonography. Comput Med Imaging Graph 26:33–42
47. Rahmim A, Schmidtlein CR, Jackson A, Sheikhbahaei S, Marcus C, Ashrafinia S, Soltani M, Subramaniam RM (2016) A novel metric for quantification of homogeneous and heterogeneous tumors in PET for enhanced clinical outcome prediction. Phys Med Biol 61:227–242
48. Shinohara RT, Crainiceanu CM, Caffo BS, Reich DS (2011) Longitudinal analysis of spatiotemporal processes: a case study of dynamic contrast-enhanced magnetic resonance imaging in multiple sclerosis. In: Johns Hopkins University, Dept. of Biostatistics Working Papers, Warking Paper 231. Ed. Cooter RD and Edlin AS. Berkeley: Bepress, pp 1–34.
49. Kirienko M, Cozzi L, Rossi A, Voulaz E, Antunovic L, Fogliata A, Chiti A, Sollini M (2018) Ability of FDG PET and CT radiomics features to differentiate between primary and metastatic lung lesions. Eur J Nucl Med Mol Imaging 45:1649–1660
50. Panth KM, Leijenaar RT, Carvalho S et al (2015) Is there a causal relationship between genetic changes and radiomics-based image features? An in vivo preclinical experiment with doxycycline inducible GADD34 tumor cells. Radiother Oncol 116:462–466
51. Kickingereder P, Burth S, Wick A, Götz M, Eidel O, Schlemmer HP, Maier-Hein KH, Wick W, Bendszus M, Radbruch A, Bonekamp D (2016) Radiomic profiling of glioblastoma: identifying an imaging predictor of patient survival with improved performance over established clinical and radiologic risk models. Radiology 280:880–889
52. Parmar C, Leijenaar RT, Grossmann P et al (2015) Radiomic feature clusters and prognostic signatures specific for lung and head & neck cancer. Sci Rep 5:11044
53. Hatt M, Tixier F, Visvikis D, Cheze LRC (2017) Radiomics in PET/CT: more than meets the eye? J Nucl Med 58:365–366
54. Hatt M, Tixier F, Pierce L, Kinahan PE, le Rest CC, Visvikis D (2017) Characterization of PET/CT images using texture analysis: the past, the present... any future? Eur J Nucl Med Mol Imaging 44:151–165
55. Leijenaar RT, Nalbantov G, Carvalho S et al (2015) The effect of SUV discretization in quantitative FDG-PET Radiomics: the need for standardized methodology in tumor texture analysis. Sci Rep 5:11075
56. van Velden FHP, Kramer GM, Frings V, Nissen IA, Mulder ER, de Langen AJ, Hoekstra OS, Smit EF, Boellaard R (2016) Repeatability of radiomic features in non-small-cell lung cancer [^{18}F]FDG-PET/CT studies: impact of reconstruction and delineation. Mol Imaging Biol 18:788–795
57. Larue R, van Timmeren JE, de Jong E et al (2017) Influence of gray level discretization on radiomic feature stability for different CT scanners, tube currents and slice thicknesses: a comprehensive phantom study. Acta Oncol 56:1544–1553
58. Altazi BA, Zhang GG, Fernandez DC, Montejo ME, Hunt D, Werner J, Biagioli MC, Moros EG (2017) Reproducibility of F18-FDG PET radiomic features for different cervical tumor segmentation methods, gray-level discretization, and reconstruction algorithms. J Appl Clin Med Phys 18:32–48
59. Razak ARA, Siu LL, Liu F et al (2010) Nasopharyngeal carcinoma: the next challenges. Eur J Cancer 46:1967–1978
60. Wong AJ, Kanwar A, Mohamed AS, Fuller CD (2016) Radiomics in head and neck cancer: from exploration to application. Transl Cancer Res 5:371–382
61. Orlhac F, Boughdad S, Philippe C, Stalla-Bourdillon H, Nioche C, Champion L, Soussan M, Frouin F, Frouin V, Buvat I (2018) A post-reconstruction harmonization method for multicenter radiomic studies in PET. J Nucl Med 59:1321–1328